

# On the prediction of liquefaction resistance of unsaturated sands

Lucia Mele\*, Alessandro Flora

DICEA, University of Napoli Federico II, Italy

## ARTICLE INFO

### Keywords:

Liquefaction  
Partial saturation  
Liquefaction specific energy  
Design of induced partial saturation (IPS)

## ABSTRACT

The increasing interest in the undrained cyclic behaviour of unsaturated soils is justified by the evidence of the beneficial effect of desaturation on liquefaction resistance and is thus strictly connected with the need to put forth sound tools to be used in the design of Induced Partial Saturation (IPS) interventions. IPS is still far from being a routine technology because of the lack of such design tools, as well as of simple technologies to obtain and preserve it on site. This paper offers a contribution to the first issue, based on the energetic interpretation of laboratory results that highlights the role of the volumetric and deviatoric components of the specific energy spent during undrained cycling on the liquefaction mechanism. Independent experimental results taken from the literature are successfully simulated using this interpretation. Then, stemming from the theoretical and experimental considerations reported in the first part of the paper, two possible approaches to calculate the desired degree of saturation of a loose sand (design goal for IPS) are introduced and discussed.

## 1. Introduction

In shallow, saturated and loose sandy soils, a seismic ground motion can cause a rapid increase of pore water pressure, with a subsequent decrease of effective stresses that may eventually lead to a loss of shear strength and to liquefaction. Since in this transient state the soil behaves as a fluid, liquefaction is a relevant cause of damage to structures and infrastructures during earthquakes. Therefore, it is of the outmost relevance to identify mitigation techniques able to tackle the risk and satisfying the requisites of soundness and reliability in design, environmental compatibility and cost effectiveness. The mitigation actions belonging to the family of ground improvement techniques (i.e. those concentrating on the ground and not on the foundations of structures) may modify soil density (compaction), composition (addition of fines or cementation), water flow patterns (drainage) or the degree of saturation (induced partial saturation, IPS). The latter is considered one of the most innovative and promising technologies against liquefaction (e.g. Refs. [1–9]), especially when the goal is to protect existing buildings that may suffer from the use of more invasive ones [10]. Recently, some in-situ trial applications of this technology have been carried out to decrease the susceptibility of liquefiable soil deposits (e.g. Refs. [11,12]).

It is well-known that partial saturation increases the liquefaction resistance because of the very low volumetric stiffness of the gaseous phase. During undrained cyclic loading, if the soil tends to contract, the volume of the gas phase decreases and consequently the pore pressure

build-up is reduced. This simple mechanism has a large effect even when the saturation degree is as high as 99%, and obviously becomes more and more relevant as the degree of saturation ( $S_r$ ) decreases. From a qualitative point of view, it can be also said that desaturation sharply reduces the volumetric stiffness  $K_{eq}$  of the equivalent pore fluid (gas plus water), as shown by the available analytical relationships (e.g. Ref. [13]).

In laboratory testing, liquefaction is usually studied through undrained cyclic triaxial or simple shear tests. Even though cyclic simple shear tests apply more realistic stress paths, cyclic triaxial tests are more popular and widely used to assess soil liquefaction potential. The results are usually interpreted in the CSR vs. N plane, being CSR the *Cyclic Stress Ratio* and N the applied number of constant amplitude stress cycles.  $N_{liq}$  is the value of N needed to reach liquefaction for a given value of CSR. For  $N = N_{liq}$ , the applied cyclic stress ratio represents the *Cyclic Resistance Ratio* CRR. The locus ( $N_{liq}$ :CRR) identifies the *Cyclic Resistance Curve*. Conventionally, it is assumed that liquefaction is triggered at 5% double strain amplitude (strain criterion) or at  $R_u = 0.90$ , being  $R_u = \Delta u / \sigma'_o$  (stress criterion), where  $\Delta u$  is the excess of pore air pressure for the specimen with positive suction measurement, otherwise it is the excess of pore water pressure [7]. In this work, the previous one will be adopted, following the considerations reported by Mele et al. [4]. In triaxial tests, CSR is defined as:

$$CSR = \frac{q_d}{2 \cdot \sigma'_c} \quad (1)$$

\* Corresponding author.

E-mail address: [lucia.mele@unina.it](mailto:lucia.mele@unina.it) (L. Mele).

<https://doi.org/10.1016/j.soildyn.2019.05.028>

Received 14 November 2018; Received in revised form 15 April 2019; Accepted 17 May 2019

0267-7261/ © 2019 The Authors. Published by Elsevier Ltd. This is an open access article under the CC BY-NC-ND license (<http://creativecommons.org/licenses/by-nc-nd/4.0/>).

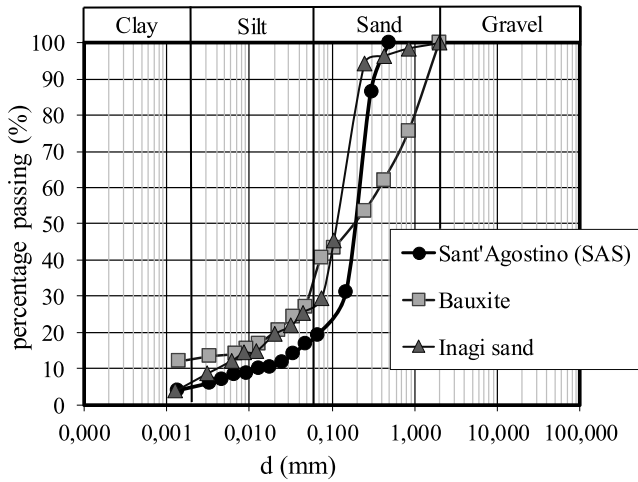


Fig. 1. Grain size distributions of the sands tested by Mele et al. [4].

where  $q_d$  is the cyclic deviatoric stress and  $\sigma'_c$  is the confining effective stress. Eq. (1) defines CSR for both saturated and unsaturated soils, provided the effective stresses are properly defined, for instance using the expression proposed by Bishop and Blight [14]:

$$\sigma'_{un} = (\sigma - u_a) + \chi \cdot (u_a - u_w) \quad (2)$$

where  $\sigma$  is the total stress and  $u_a$ ,  $u_w$  e  $\chi$  are respectively the pore air pressure, the pore water pressure and the material parameter accounting for the effect of the degree of saturation. The term  $(\sigma - u_a)$  is called “net stress”, while  $(u_a - u_w)$  is the “matric suction” ( $s$ ). Several definitions of the parameter  $\chi$  have been introduced by previous researchers [14–16], in this paper, the parameter  $\chi$  is assumed equal to the degree of saturation  $S_r$  ( $\leq 100\%$ ) as shown by Refs. [17,18]. The difference between the undrained cyclic behaviour of saturated and unsaturated soils is the existence of volumetric strains  $\varepsilon_v$  in the latter caused by the compression of the gas phase and, in a minor part, by the increase of its solubility in the liquid phase connected to the increase of pressure, as ruled by Henry's law.

Testing on three fine sands differing by gradation and mineralogical origin (Fig. 1 and Table 1), Mele et al. [4] showed that during undrained cyclic triaxial loading of loose unsaturated sands, whatever the applied CSR,  $\varepsilon_v$  increases to a final value  $\varepsilon_{v,fin}$  at liquefaction which depends only on the initial state, defined for instance via the degree of saturation ( $S_{r0}$ ), the void ratio ( $e_0$ ) and the initial net stress  $(\sigma - u_a)_0$ . Considering the deformation process isothermal and applying Boyle and Mariotte law, the final volumetric strain at a constant confining total stress  $\sigma_c$  and with an initial air pressure  $u_{a,0}$  can be written as [4,19]:

$$\varepsilon_{v,fin} = \frac{e_0}{1 + e_0} \cdot (1 - S_{r0}) \cdot \left(1 - \frac{u_{a,0}}{\sigma_c}\right) \quad (3)$$

Eq. (3) holds for any material that, during the cyclic loading process, experiences positive volumetric strains (i.e. compression). Therefore, it cannot be applied to very dense soils, which may experience dilative behaviour. Since this research aims to study the behaviour of

loose, liquefiable soils, this is only a theoretical drawback, and does not limit the applicability of the approach.

The relationship between the initial state and the volumetric deformations in undrained cyclic tests is shown in the  $\varepsilon_v - \sigma'_{un}$  plane (Fig. 2a) for the experimental tests reported by Mele et al. [4]. Since for bauxite the minimum and maximum void ratio were not evaluated (Table 1), the degree of compaction  $D_c$  is reported for it in the figure, defined as the ratio between the dry density of the specimen ( $\rho_d$ ) and the maximum dry density ( $\rho_{dmax} = 1.70 \text{ g/cm}^3$  in this case).

Fig. 2a indicates that, for the three tested sands, the average curve for each value of  $S_r$  is the same for all the tests. Interestingly, in a non-dimensional plane ( $\sigma'_{un}/\sigma'_{un,0} - \varepsilon_v/\varepsilon_{v,fin}$ , Fig. 2b) a unique curve is obtained for all the experimental results, having the expression:

$$\frac{\sigma'_{un}}{\sigma'_{un,0}} = 1 - \left(\frac{\varepsilon_v}{\varepsilon_{v,fin}}\right)^{1.7} \quad (4)$$

Even though it is expected that some differences may appear at much higher confining stresses because of the increased gas solubility, it must be highlighted that on site liquefaction is a critical mechanism for the possible effects on structures at ground level only when it takes place in shallow layers (i.e. at low confining stresses, say for  $\sigma'_{un} \leq 100 \text{ kPa}$ ). Therefore, from a practical point of view and with this limitation, Mele et al. [4] suggest that it is reasonable to consider eq. (4) as a general law, valid for all possible intrinsic and state properties of different soils at low confining stresses.

## 2. The use of specific energy to predict the liquefaction resistance of unsaturated soils

In recent years, energetic concepts are increasingly developing, with the main aim to determine the parameters that could better define liquefaction potential of a soil deposit [20–22]. The energetic approaches seem to be very promising, due to the fact that the dissipated energy required for the onset of liquefaction is practically independent of the applied loading pattern (uniform and non-uniform) [23,24] and type of test performed (cyclic torsional, cyclic triaxial, cyclic simple shear or centrifuge tests) [25,26]. All these studies refer to saturated sandy soils, highlighting a strong dependence of dissipated energy on excess pore pressure ratio [21,27,28]. On the contrary, very little has been done on the effect of energy on unsaturated sandy soils (e.g. Ref. [4]); but only with reference to the effect of the volumetric component).

In this paper, an energetic interpretation of the results of unsaturated tests has been done considering both the volumetric and deviatoric components. A partially saturated soil can be considered as a three-phases thermodynamic system. In order to quantify the energy spent by the soil specimen during the pore pressure build-up process till liquefaction during laboratory testing, four hypothesis will be introduced:

- The process is isothermal (i.e. no heat is generated or lost during the test);
- The mass of the system is constant (i.e. no increase or decrease of the mass of air, water or soil in the specimen during the test);
- The system is thermodynamically open (i.e. within the specimen the deformation process implies internal flows of air and water);
- The pore gas (air) can be treated as an ideal gas.

The total specific energy of deformation  $E_{tot}$  needed to reach liquefaction can be seen as the sum of two components:

$$E_{tot,liq} = E_{v,liq} + E_{s,liq} \quad (5)$$

where  $E_{v,liq}$  is the volumetric specific energy and  $E_{s,liq}$  is the deviatoric specific energy to reach liquefaction.

The role played by these two components within the liquefaction phenomenon will be discussed in the following.

Table 1

Physical properties of the sands tested by Mele et al. [4].

Material Property	Sant'Agostino (SAS)	Bauxite	Inagi sand
Fines Content ( $d < 0.075 \text{ mm}$ ) (%)	20.0	40.6	29.5
Specific Gravity, $G_s$	2.674	2.642	2.656
D50 (mm)	0.200	0.200	0.115
$e_{max}$	1.01	–	1.645
$e_{min}$	0.37	–	0.907
$U_c$	16.7	400	30.0

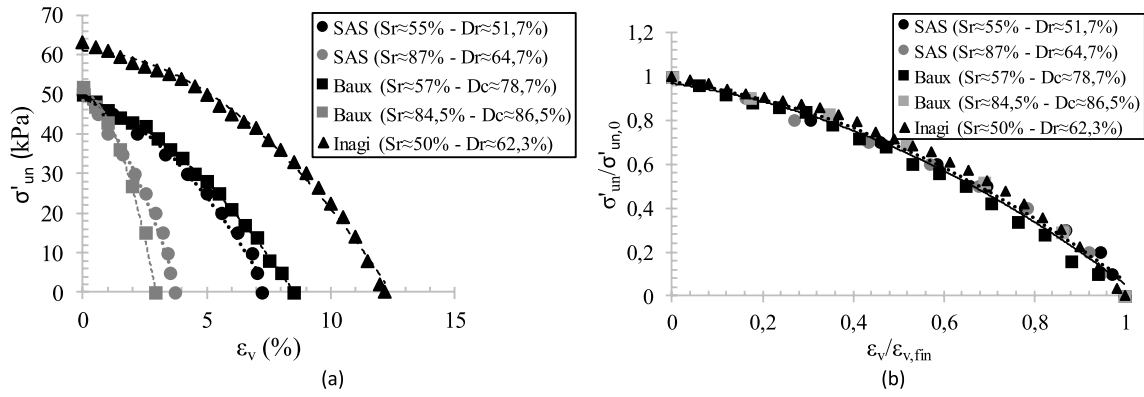


**Fig. 2.** Effective stress vs. volumetric strain (a) and dimensionless effective stress vs. dimensionless volumetric strain (b) for some of the tests reported by Mele et al. [4]. In all cases, the confining effective stress was in the range 50–60 kPa.

The volumetric specific energy can be seen as the sum of three components [4]:

$$E_{v,liq} = E_{v,sk,liq} + E_{w,liq} + E_{air,liq} \quad (6)$$

$E_{v,sk,liq}$ ,  $E_{w,liq}$  and  $E_{air,liq}$  represent the specific work done respectively to cause the deformation of the soil skeleton, the flow of water and the flow of air into the pores network. They can be expressed as:

$$E_{v,sk,liq} = \int_0^{\varepsilon_{v,liq}} [(\sigma - u_a) + sS_r] \cdot d\varepsilon_v \quad (7)$$

$$E_{w,liq} = - \int_{S_{r0}}^{S_{r,liq}} \frac{e(S_r)}{1 + e(S_r)} s(S_r) \cdot dS_r \quad (8)$$

$$E_{air,liq} = \frac{e_0}{1 + e_0} (1 - S_{r,0}) u_{a,liq} d(\ln \rho_{a,liq}) \quad (9)$$

$E_{v,sk,liq}$  depends on the stress state ( $\sigma'_{un}$ ) and on the initial void ratio  $e_0$  ( $E_{v,sk,liq} = f(\sigma'_{un}, e_0)$ ), while it depends neither on CSR nor on  $N_{liq}$ . Obviously,  $E_{v,sk,liq} = 0$  for undrained tests on saturated soils. The integral of eq. (7) represents the area of the average curve  $\sigma'_{un}-\varepsilon_v$  (i.e. Fig. 2a) for a specific soil state. The integration extremes for the volumetric strains have to be assigned to calculate  $E_{v,liq}$ . These are 0 and  $\varepsilon_{v,liq}$ , respectively corresponding to the effective stresses (Bishop's notation)  $\sigma'_{un,0}$  and  $\sigma'_{un,liq}$ . The latter is the value of the effective stress at liquefaction and is not nil because of the conventional definition of

liquefaction ( $\varepsilon_{DA} = 5\%$ ). It can be calculated as a function of the initial degree of saturation  $S_{r0}$  using the following equation:

$$\frac{\sigma'_{un,liq}}{\sigma'_{un,0}} = -2 \cdot 10^{-4} S_{r0}^2 + 2 \cdot 10^{-2} S_{r0} + 0.1 \quad (10)$$

which is the best fitting curve of the experimental data presented by Mele et al. [4] and reported in Table 2.

For saturated soils ( $S_{r0} = 100\%$ ), the stress and strain criteria give the same results in term of  $N_{liq}$ , as shown by Mele et al. [4]. In Fig. 3, for  $S_{r0} = 100\%$  it is found that  $\sigma'_{un,liq}/\sigma'_{un,0} = 0.1$ . This is consistent with the definition of liquefaction according to the stress criterion, (i.e. liquefaction occurs at  $R_u = 0.90$ ), even though the results were interpreted in terms of the strain criterion.

$E_{w,liq}$  is the specific volumetric energy of water and it is due to the change of water content. For sands having a high degrees of saturation (i.e. having a continuous water phase within the network of pores), the variation of suction  $s$  during the cyclic undrained tests is generally very low [4]. Then, for the sake of simplicity, the specific volumetric energy of water (eq. (8)) can be calculated assuming for the suction  $s$  a constant, average value without introducing a relevant error.

$E_{air,liq}$  describes the effect of pressure variation in the gas phase, and poses no problems in calculation.

Once the volumetric components have been defined, it is necessary to quantify the specific deviatoric energy of the soil skeleton spent to liquefaction,  $E_{s,liq}$ , connected to distortional strains  $\varepsilon_s$ . From a physical

**Table 2**  
State properties and energetic components calculated for the tests reported by Mele et al. [4].

Test	Material	$\sigma'_{un}$ (kPa)	$e_0$	$S_{r0}$ (%)	$E_{v,sk,liq}$ (J/m <sup>3</sup> )	$E_{w,liq}$ (J/m <sup>3</sup> )	$E_{air,liq}$ (J/m <sup>3</sup> )	$E_{v,liq}$ (J/m <sup>3</sup> )	$E_{v,liq,ave}$ (J/m <sup>3</sup> )	$E_{s,liq}$ (J/m <sup>3</sup> )
U_SA1	SAS	49.6	0.71	53.0	1700	0	574	2274	2280	4257
U_SA2	SAS	50.5	0.67	54.0	1700	-40.0	572	2232		4721
U_SA3	SAS	48.9	0.67	56.0	1700	-20.0	654	2334		7534
U_SA4	SAS	50.5	0.61	90.0	1095	0	106	1201	1192	3545
U_SA5	SAS	49.8	0.60	81.5	1095	0	210	1305		7042
U_SA6	SAS	49.8	0.59	87.2	1095	0	54	1149		3267
U_SA7	SAS	49.9	0.58	86.7	1095	0	13	1232		3043
U_SA8	SAS	48.8	0.59	87.6	1095	0	49	1144		2486
U_SA9	SAS	50.4	0.61	88.5	1095	0	27	1122		1427
U_BA1	Bauxite	51.9	0.91	58.0	2347	-138	1070	3279	3087	21638
U_BA2	Bauxite	56.3	0.92	56.0	2347	-167	991	3172		13308
U_BA3	Bauxite	51.8	0.94	56.0	2347	-109	572	2811		7987
U_BA4	Bauxite	47.4	0.76	84.0	933	106	145	1185	1200	1417
U_BA5	Bauxite	48.4	0.75	85.0	933	127	156	1215		3622
U_IN1	Inagi	62.2	1.20	49.0	3452	-581	1141	4012	4035	14492
U_IN2	Inagi	64.2	1.22	48.0	3452	-655	1323	4120		15902
U_IN3	Inagi	62.3	1.14	52.0	3452	-661	1182	3973		10306

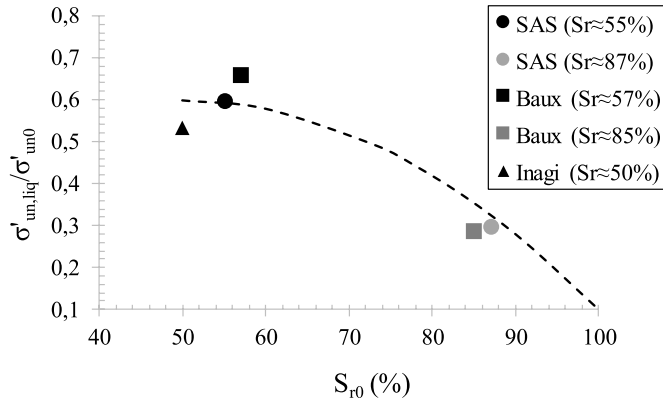


Fig. 3. Experimental values of  $\sigma'_{un,liq}/\sigma'_{un,0}$  and  $S_{r0}$  [4], along with a best fitting curve (eq. (10)).

point of view,  $E_{s,liq}$  is the sum of the areas of all the cycles in the  $\varepsilon_s:q$  plane ( $D_{cyc}$  in Fig. 4 for a single cycle) up to liquefaction (defined in terms of strains). Formally, for each cycle the energy is defined as:

$$E_{s,sk,cyc} = \int_{D_{cyc}} dq \cdot d\varepsilon_s \quad (11a)$$

And therefore:

$$E_{s,sk,liq} = \sum_{N_{cyc}=1}^{N_{cyc}=N_{liq}} E_{s,sk,cyc} \quad (11b)$$

Because of its definition,  $E_{s,liq}$  is strictly related to soil damping, and it thus quantifies the amount of energy dissipated during the distortional cyclic path. Therefore, it depends on soil properties, soil state and cyclic stress amplitude CSR. Since no distortional strains are generated by the work input into the liquid and gas phases, eq. (11b) represents the only distortional energetic contribution ( $E_{s,sk,liq} = E_{s,liq}$ ).

The role of specific volumetric and deviatoric energies will be analysed in the following using the previously recalled experimental results obtained by Mele et al. [4]. To this aim, the state properties and specific energetic components of all these tests are reported in Table 2.

Since for design issues the liquefaction resistance in simple shear conditions ( $CRR^{css}$ ) is needed, when using triaxial results it is custom to calculate it correcting the one referred to triaxial conditions ( $CRR^{ctx}$ ) as [29]:

$$CRR^{css} = c_r \cdot CRR^{ctx} \quad (12a)$$

where  $c_r$  is:

$$c_r = \frac{2 \cdot (1 + 2K_0)}{3\sqrt{3}} \quad (12b)$$

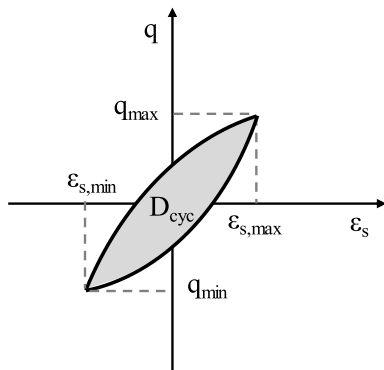


Fig. 4. Definition of the specific deviatoric energy  $E_{s,sk}$  for a single cycle in the  $q:\varepsilon_s$  plane [4].

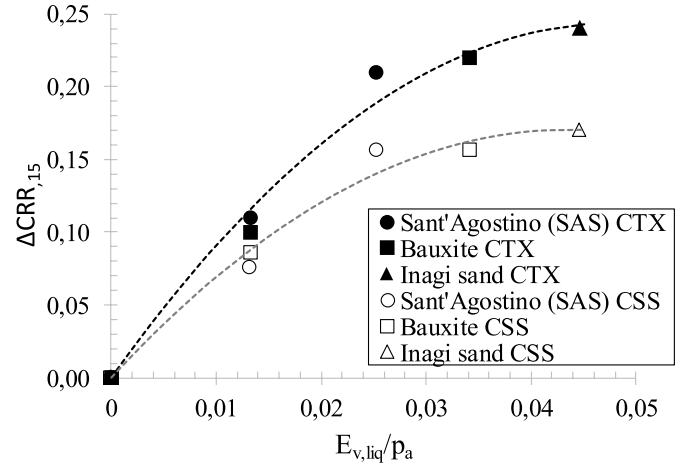


Fig. 5. Ratio between unsaturated and saturated liquefaction resistance at  $N_{cyc} = 15$  ( $\Delta CRR_{15}^{ctx}$  and  $\Delta CRR_{15}^{css}$ ) versus  $E_{v,liq}/p_a$ .

in eq. (12b)  $K_0$  is the coefficient of earth pressure at rest, evaluated as  $K_0 = 1 - \sin \phi_p$ , where  $\phi_p$  is the peak friction angle. In this work, the value  $\phi_p = 35^\circ$  was used for Sant'Agostino and Inagi sands, while  $\phi_p = 36^\circ$  was used for Bauxite. It has to be remarked that the value of  $\phi_p$  for Sant'Agostino sand was experimentally measured, while the values for the other two sands were estimated based on their gradings and mineralogies. In the range of expected values for sands, variations of  $\phi_p$  have a minor effect on  $c_r$ , so this assumption does not have any relevant quantitative effect, thus being acceptable.

## 2.1. The role of the specific volumetric energy to liquefaction, $E_{v,liq}$ – approach 1

The volumetric specific energy  $E_{v,liq}$  (eqs. (6)–(9)) is a function of the initial values of the effective confining stress (Bishop notation), of the void ratio and of the degree of saturation ( $E_{v,liq} = E_{v,liq}(\sigma'_0, e_0, S_{r0})$ ), and increases from zero (for saturated soils) as  $S_r$  decreases. In this sense,  $E_{v,liq}$  may be seen as a synthetic state variable ruling the increment of liquefaction resistance of sands (at low confining stresses) from  $CRR_s$  ( $S_r = 100\%$ ) to  $CRR_{un}$  ( $S_r < 100\%$ ). In Fig. 5, the differences  $\Delta CRR^{ctx} = CRR_{un}^{ctx} - CRR_s^{ctx}$  and  $\Delta CRR^{css} = CRR_{un}^{css} - CRR_s^{css}$  (eqs. (12a) and (12b)) calculated for  $N_{liq} = 15$  are plotted versus  $E_{v,liq}$  for the three tested sands (Fig. 1). A clear relationship between  $\Delta CRR^{ctx}$  (or  $\Delta CRR^{css}$ ) and  $E_{v,liq}$  is observed for all the tested initial state conditions, confirming that an increase in the specific volumetric energy spent to liquefaction corresponds to an increase in liquefaction resistance, with a rate that seems to reduce as  $E_{v,liq}$  increases. Based on the experimental results reported in Fig. 5, the relationships between  $E_{v,liq}$  and  $\Delta CRR_{N_{liq}}^{ctx}$  and  $\Delta CRR_{N_{liq}}^{css}$  (for  $N_{liq} = 15$ ) can be expressed as:

$$\Delta CRR_{N_{liq}}^{ctx} = -105.7 \cdot \left( \frac{E_{v,liq}}{p_a} \right)^2 + 10.16 \cdot \frac{E_{v,liq}}{p_a} \quad (13a)$$

$$\Delta CRR_{N_{liq}}^{css} = -89.6 \cdot \left( \frac{E_{v,liq}}{p_a} \right)^2 + 7.81 \cdot \frac{E_{v,liq}}{p_a} \quad (13b)$$

In which the atmospheric pressure  $p_a$  has been introduced to make the relationship non dimensional. Fig. 6 (a for triaxial tests and b for corrected experimental data) indicate that, in the range of  $N_{liq}$  of practical interest ( $N_{liq} \leq 20$ ), the same conclusion can be extended to all values of  $N_{liq}$ :  $\Delta CRR^{ctx}$  does not depend on  $N_{liq}$  but only on  $E_{v,liq}$ . In other words, for  $N_{liq} \leq 20$ ,  $\Delta CRR$  can be univocally related to  $E_{v,liq}$ , and therefore desaturation leads to a simple translation towards higher values of CRR of the liquefaction resistance curve, without appreciable change in shape. This procedure (approach 1) will be tested on literature data in §4.1.

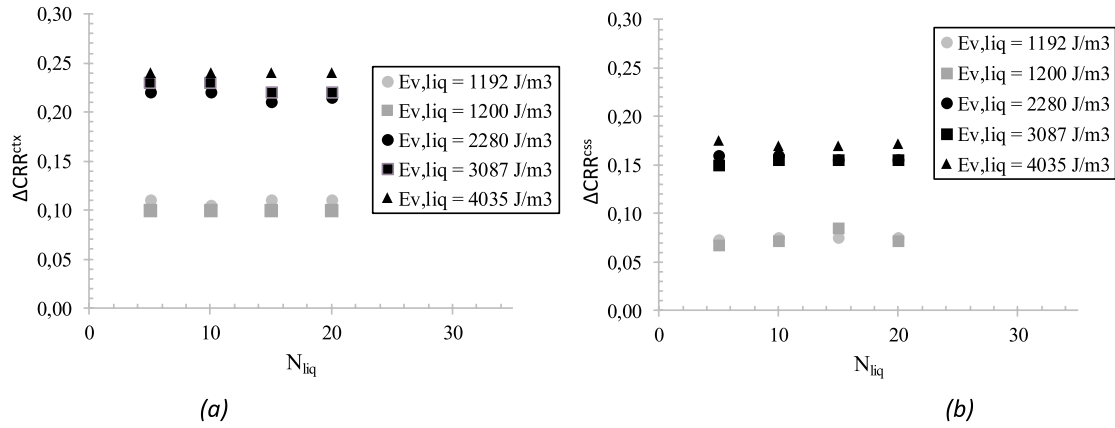


Fig. 6.  $\Delta CRR^{ctx}$  versus  $N_{liq}$  (a);  $\Delta CRR^{css}$  versus  $N_{liq}$  (b).

## 2.2. The role of the specific deviatoric energy to liquefaction, $E_{s,liq}$

As mentioned above, the specific deviatoric energy to liquefaction  $E_{s,liq}$  can be evaluated from eqs. (11a) and (11b) as the sum of the areas of all cycles in the  $\varepsilon_s:q$  plane (Fig. 4). Therefore (unlike  $E_{v,liq}$ ) it depends on the applied cyclic stress (CSR) and on the number of cycles to liquefaction ( $N_{liq}$ ).

For some of the unsaturated tests reported by Mele et al. [4] (Table 1), the current specific deviatoric energy  $E_s$  has been evaluated along the whole path to liquefaction and after (Figs. 7–9) to show its evolution.

The figures indicate that in the first cycles the relationship  $N_{cyc}:E_s$  is roughly linear, with a slope which depends on the applied CSR and on soil state. This means that, for each test, the specific deviatoric energy spent in each of these first cycles is roughly the same, i.e. no significant change in the shape of each of them is taking place. Approaching liquefaction, shear strains and damping sharply increase, and so does  $E_s$ . The onset of liquefaction ( $N_{cyc} = N_{liq}$ ,  $E_s = E_{s,liq}$ , as conventionally evaluated for  $\varepsilon_{DA} = 5\%$ , and indicated with vertical arrows in Figs. 7–9) corresponds to the highest gradient in the  $N_{cyc}:E_s$  plot for all tests, except for U\_BA1 and U\_BA2 (Fig. 8a). For these two tests, according to the strain criterion liquefaction occurs at a value of  $N_{cyc}$  higher than that at which the gradient is the highest. The results of tests U\_BA1 and U\_BA2 are related to the sudden onset of large plastic strains before reaching liquefaction (maximum gradient in Fig. 8a, sharp increase of  $\varepsilon_a$  in Fig. 10a). Analysing in detail the results of these two tests, it can be noted (Fig. 10a) that the axial strains do not cycle around zero, with a sort of ratcheting mechanism towards the negative values likely related to a shear failure in extension prior to the attainment of liquefaction. Fig. 10b reports the results of test U\_BA5, on the same material

(bauxite), showing that in this as in all the other cases but tests U\_BA1 and U\_BA2, cycles are much more symmetric around the  $N_{cyc}$  axis, and shear strains rapidly increase in correspondence of pore pressure build-up leading to liquefaction. A confirmation is given by Fig. 10c and d, in which  $R_u$  versus  $N_{cyc}$  is plotted for the same tests: for U\_BA1 and U\_BA2, in fact, liquefaction in terms of pore pressure increments takes place at a number of cycles much higher than that corresponding to the strain criterion (Fig. 10a and c), while for test U\_BA5 the two criteria give the same result ( $N_{liq} = 7-8$ , Fig. 10b and d).

Figs. 7–9 also indicate that the values of  $E_{s,liq}$  increase as the degree of saturation decreases and as the applied cyclic stress CSR decreases.

Fig. 11a reports the same experimental results in the  $E_{s,liq}:CRR^{ctx}$  plane, confirming that the value of CRR attained in each test, for each soil and initial state, is uniquely related to  $E_{s,liq}$ . Since state conditions of unsaturated soils during cycling tests are well represented by  $E_{v,liq}$ , a much more general interpretation can be obtained by plotting the experimental data in the normalized plot in Fig. 11b, in which a unique, non linear relationship links  $E_{s,liq}$  to the term  $(CRR^{ctx} \cdot (1 - 5 \cdot E_{v,liq}/p_a))^{10}$ , where the exponent has been calibrated to obtain the best fitting of the experimental data with the equation:

$$E_{s,liq} = 0.297 \cdot p_a \cdot e^{-16.7 \cdot CRR^{ctx} \cdot \left(1 - 5 \cdot \frac{E_{v,liq}}{p_a}\right)^{10}} \quad (14a)$$

Similarly, considering the cyclic resistance ratios in simple shear conditions (eqs. (12a) and (12b)) a best fitting relationship is found as:

$$E_{s,liq} = 0.300 \cdot p_a \cdot e^{-23.7 \cdot CRR^{css} \cdot \left(1 - 5 \cdot \frac{E_{v,liq}}{p_a}\right)^{10}} \quad (14b)$$

Summing up all the experimental evidences, it may be concluded that - for a given soil -  $E_{v,liq}$  represents the state variable defining the

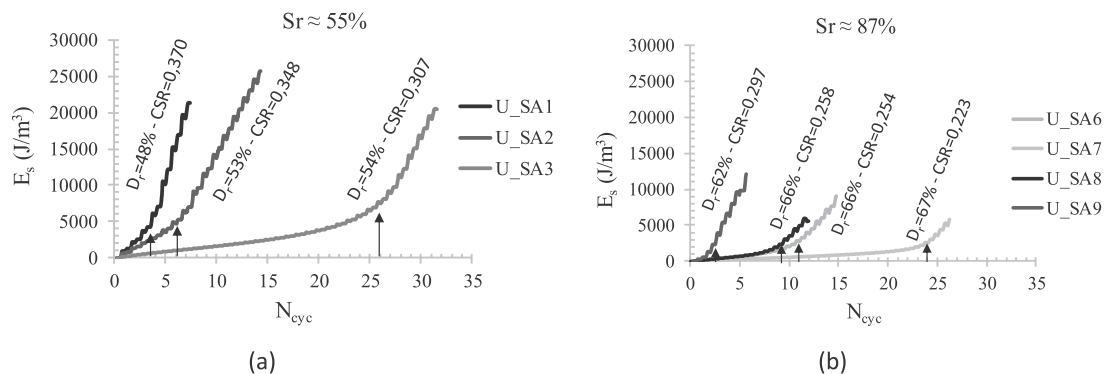
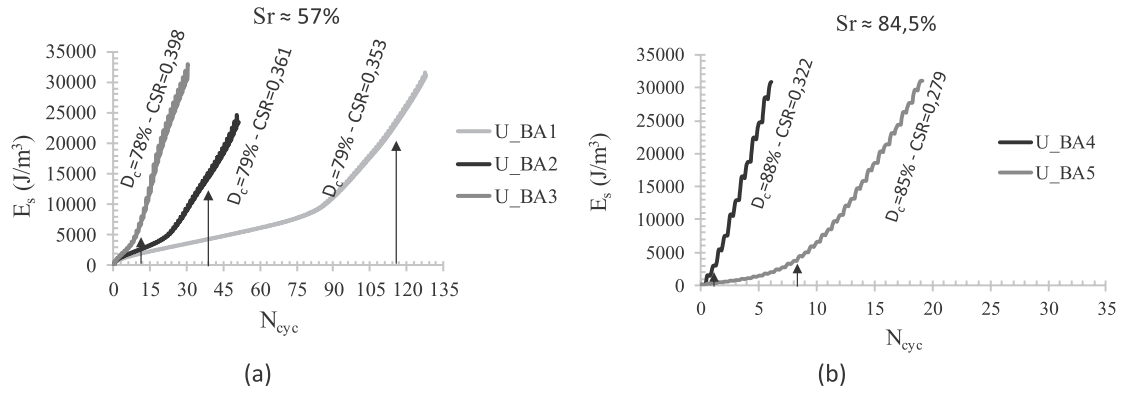
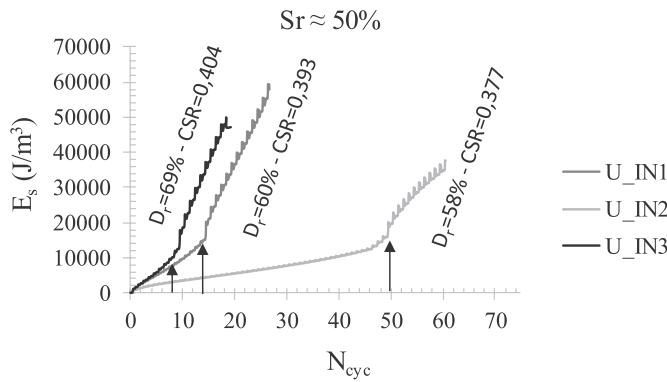


Fig. 7.  $E_s$  versus  $N_{cyc}$  along the cyclic undrained tests on unsaturated Sant'Agostino sand [4] for a low (a) and high (b) degree of saturation. Liquefaction triggering is indicated by the vertical arrows.





**Fig. 8.**  $E_s$  versus  $N_{cyc}$  along the cyclic undrained tests on unsaturated Bauxite [4] for a low (a) and high (b) degree of saturation. Liquefaction triggering is indicated by the vertical arrows.



**Fig. 9.**  $E_s$  versus  $N_{cyc}$  along the cyclic undrained tests on unsaturated Inagi sand [4]. Liquefaction triggering is indicated by the vertical arrows.

modification of position (increase of resistance) of the liquefaction curve due to unsaturation (Fig. 5), while  $E_{s,liq}$  is the energetic variable that, given the value of  $E_{v,liq}$ , defines the cyclic resistance CRR (and therefore also the number of cycles to liquefaction  $N_{liq}$ ).

### 2.3. The normalized cyclic resistance curve based on total specific energy – approach 2

In the attempt to find a relationship between the specific energy spent to liquefaction and the cyclic resistance ratio CRR, Mele et al. [4] proposed a relationship between  $CRR/(E_{v,liq})^{0.5}$  and  $N_{liq}$ . In this paper, based on the above reported evidences, the contribution of the specific deviatoric energy is also accounted for, and the experimental results are reported in the plane  $CRR^{ctx}/(1 + E_{tot,liq}/p_a)^6$  versus  $N_{liq}$  (Fig. 12a), where  $E_{tot,liq}$  is the sum of the volumetric and the deviatoric energies spent to liquefaction (eq. (5)). In Fig. 12b the normalized cyclic resistance curve of the triaxial data are compared with corrected data through Castro correlation (eqs. (12a) and (12b)).

The best fitting of the experimental results in Fig. 12a is:

$$\frac{CRR^{ctx}}{\left(1 + \frac{E_{tot,liq}}{p_a}\right)^6} = -0.039 \cdot \ln(N_{liq}) + 0.285 \quad (15a)$$

Which can be transformed in simple shear conditions (eqs. (12a) and (12b)) as:

$$\frac{CRR^{css}}{\left(1 + \frac{E_{tot,liq}}{p_a}\right)^6} = -0.028 \cdot \ln(N_{liq}) + 0.202 \quad (15b)$$

Eqs. (15) assume that whole the considered experimental results

may be analysed together, thus implicitly assuming that the only influent parameter to quantify the liquefaction resistance curve is the total energy. This is true only if there is no other relevant effect, like for instance soil grading. Actually, the experimental results reported in Fig. 12a seem to indicate that such a dependency may exist, as the finer soil (Inagi) plots on the lower part of the graph, while the coarser one (Bauxite) on the upper one. However, the experimental results are not sufficient to introduce explicitly such a dependency. With this limitation, eqs. (14) may be seen as a synthetic way to express the cyclic resistance of unsaturated fine sands accounting for the specific total energy spent to liquefy ( $E_{tot,liq}$ ). The use of the total specific energy allows to plot the CRR- $N_{liq}$  curve of unsaturated soils without knowing the one in saturated conditions, while by using only the specific volumetric component of the energy (eq. (13)) the latter is needed.

Eq. (15a) has been calibrated on experimental data having a limited range of void ratios and confining stresses. Other tests must be carried out to confirm the validity of eq. (15a) and eq. (15b) out of the tested ranges of state properties, and to check its possible dependency on grain size distribution within the broad family of fine sands. However, it has to be emphasized again that liquefaction occurs in loose sand (low  $D_r$ ) and at shallow depths (low confining stresses). Therefore, even though the curve of Fig. 12b (eq. (15b)) cannot be intended as a general law for all possible soils states, it can be of extreme usefulness to predict the effects of induced partial saturation in the conditions of maximum practical interest on site, as shown in §4.2.

In the following, the consistency of the two possible approaches will be tested on independent literature data.

### 3. Procedures to evaluate the liquefaction resistance of unsaturated soils on site

The experimental evidences of the role played by the energetic components  $E_{v,liq}$  and  $E_{s,liq}$  allow to propose two simple and straightforward approaches (previously defined approach 1 and approach 2) to plot the liquefaction resistance curve of unsaturated soil on site (in simple shear conditions) for a given material and initial state ( $\sigma'_{un0}$ ,  $e_0$ ,  $S_{r0}$ ). The parameters of the equations proposed in this paper were calibrated on loose sands and low confining pressures, so the models hereafter presented allow to simulate the cyclic resistance curves of unsaturated soil under these conditions. The steps to calculate the two components  $E_{v,liq}$  and  $E_{s,liq}$  are the following:

Calculation of the volumetric specific energy.

1. Once the initial stress state, void ratio and saturation degree ( $\sigma'_{un0}$ ,  $e_0$ ,  $S_{r0}$ ) are known, from eq. (3) the final volumetric deformation of the soil,  $\epsilon_{v,fin}$  can be calculated.
2. Known  $\epsilon_{v,fin}$ , the regression curve reported in Fig. 2b (eq. (4)) allows

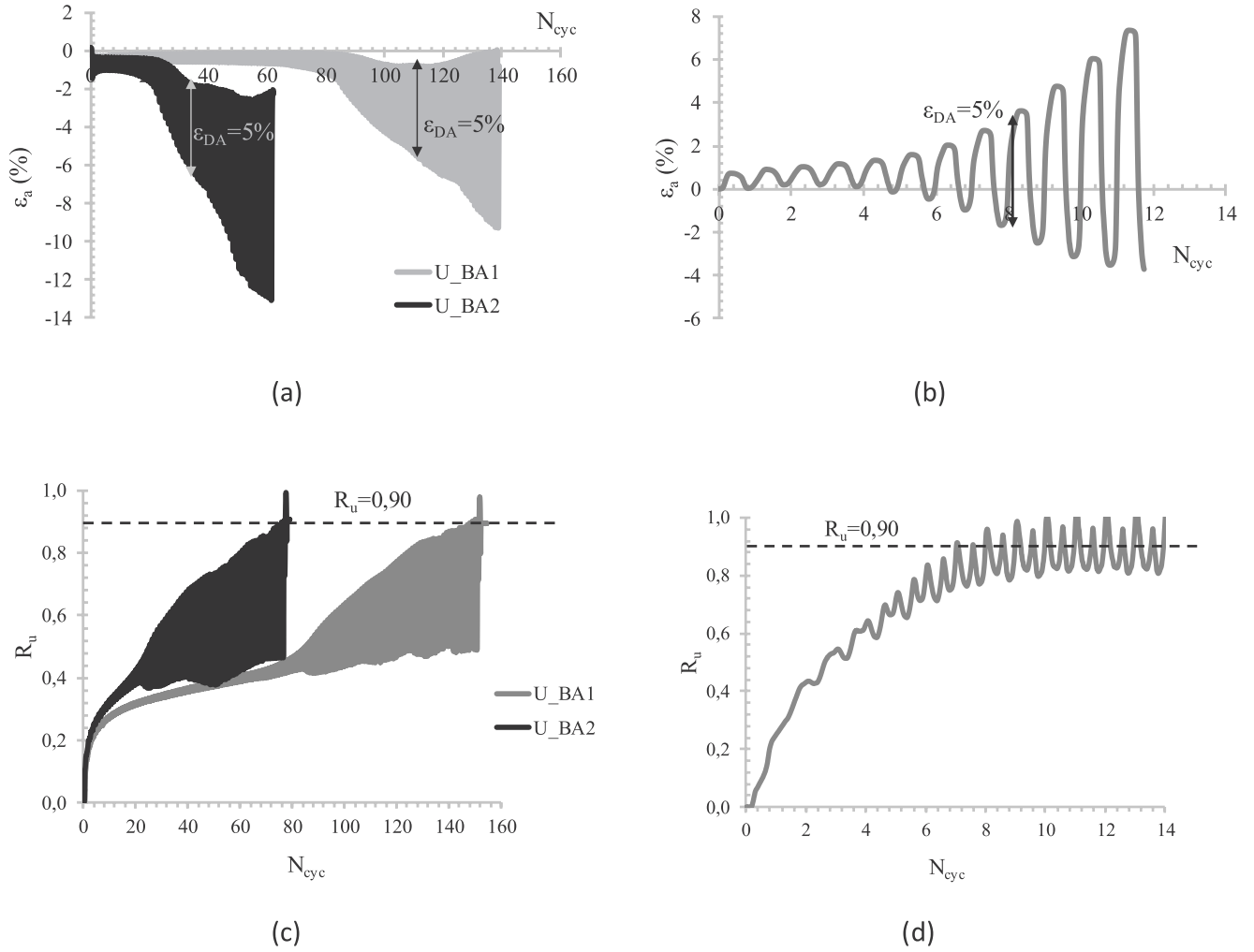


**Figure 10.**  $\varepsilon_a$  versus  $N_{cyc}$  for bauxite: U\_BA1 and U\_BA2 (a) and U\_BA5 (b);  $R_u$  versus  $N_{cyc}$  for bauxite: U\_BA1 and U\_BA2 (c) and U\_BA5 (d) [4].

to obtain the analytical relationship  $\sigma' - \varepsilon_v$  along the cycling loading path for the specific considered case. In order to calculate the component of the specific volumetric energy related to soil skeleton deformation  $E_{v,sk,liq}$  (eq. (7)), the integration extremes for the volumetric strains have to be known. As mentioned above (§2)  $\varepsilon_{v,liq}$  corresponds to  $\sigma'_{un,liq}$ , which can be found from eq. (10) once  $\sigma'_{un,0}$  and  $S_{r,0}$  are known. The volumetric strain at liquefaction  $\varepsilon_{v,liq}$  can be finally calculated using eq. (4).

- Having the water retention curve, eq. (8) allows to calculate  $E_{w,liq}$ . Again, the integration extremes have to be assigned. Based on the experimental evidences reported by Mele et al. [4]; the value of the degree of saturation at liquefaction  $S_{r,liq}$  can be simply assigned as  $S_{r,liq} = S_{r,0} + 0.08$ .
- The volumetric specific energetic component of air flow to liquefaction ( $E_{air,liq}$ , eq. (9)) can be calculated using the regression curve of Fig. 2b: once the state at liquefaction is known in terms of effective stress  $\sigma'_{un,liq}$  (Bishop's notation) as indicated at step 2, the corresponding value of air pressure can be calculated, from eq. (16) because  $\sigma_{liq}$ ,  $S_{r,liq}$  and  $s_{liq}$  are known.

$$u_{a,liq} = (\sigma_{liq} - \sigma'_{un,liq}) + S_{r,liq} \cdot s_{liq} \quad (16)$$

Similarly, since  $\varepsilon_{v,liq}$  is known, the value of  $\rho_{a,liq}$  can be calculated (because the mass of air within the specimen is known and constant).

- The total volumetric component of the specific energy  $E_{v,liq}$  can be then computed using eq. (6), based on what has been obtained in the

steps from 1 to 4.

Calculation of the deviatoric and total specific energy.

- Since  $E_{v,liq}$  is known, once the cyclic stress CSR (expected earthquake) is assigned  $E_{s,liq}$  can be calculated from eq. (14b) (Fig. 11c).
- $E_{tot,liq}$  can be calculated as the sum of the two components ( $E_{tot,liq} = E_{v,liq} + E_{s,liq}$ ).

With approach 1 (§2.1), it is necessary to know the cyclic resistance curve in saturated conditions ( $CRR_s^{css} - N_{liq}$ ) and the soil water retention curve (relationship between the degree of saturation  $S_r$  and suction  $s$ ) to calculate  $E_{v,liq}$  (steps 1 to 5) and therefore  $\Delta CRR^{css}$  (eq. (13b), Fig. 5). Then, the cyclic resistance curve in unsaturated conditions can be obtained by just  $\Delta CRR^{css}$  to  $CRR_s^{css}$ :

$$CRR_{un}^{css}(N_{liq}) = CRR_s^{css}(N_{liq}) + \Delta CRR^{css} \quad (17)$$

With approach 2 (§2.3), the knowledge of the saturated liquefaction resistance curve is not needed, but the deviatoric specific energy has to be calculated and added to the volumetric one to obtain the total specific energy (steps 6 and 7). Using the correlation (eq. (13b)) between  $CRR^{css}/(1 + E_{tot,liq}/p_a)^6$  and  $N_{liq}$ , assuming  $CSR = CRR^{css}$ , the corresponding value of  $N_{liq}$  is obtained. By repeating the procedure from step 1 to 8 for different values of CRR, the cyclic resistance curve for cyclic simple shear condition can be finally obtained with approach 2.

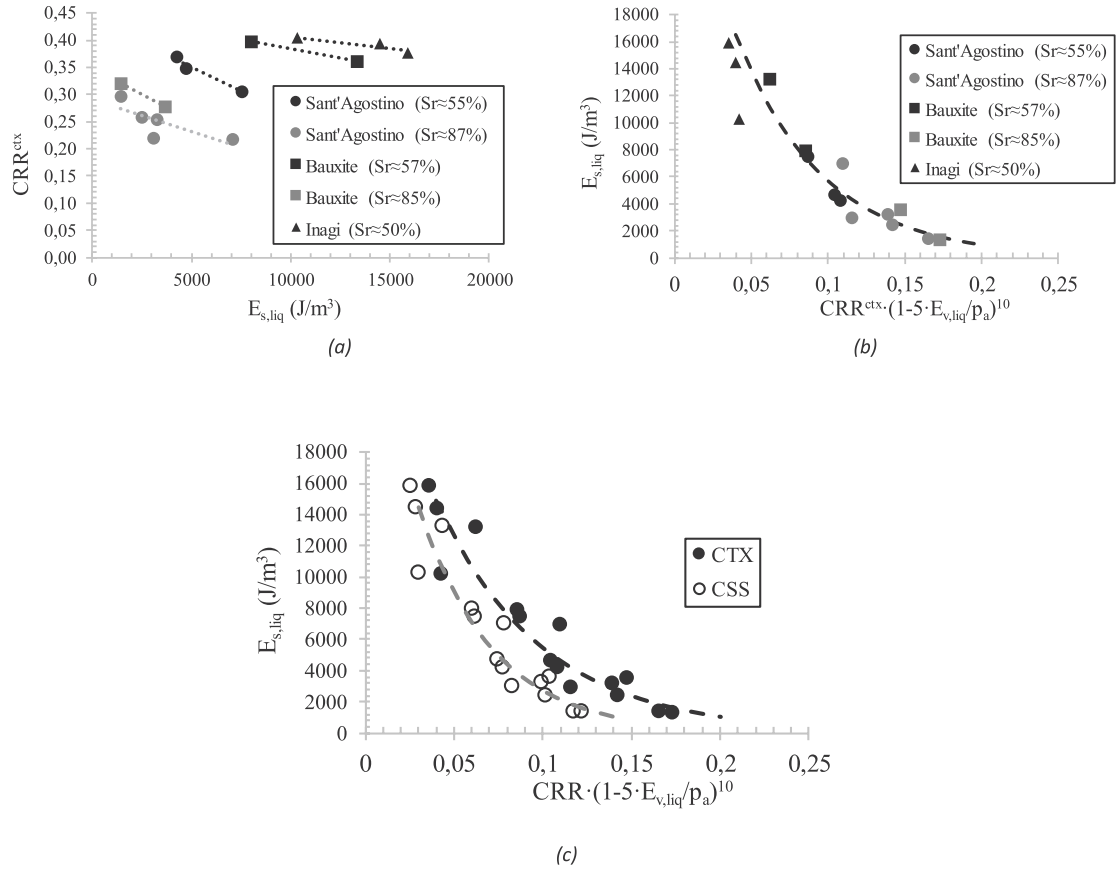


Fig. 11.  $CRR^{ctx}$  vs  $E_{s,liq}$  (a);  $CRR^{ctx} \cdot (1 - 5 \cdot E_{v,liq} / p_a)^{10}$  vs  $E_{s,liq}$  (b); Cyclic triaxial and corrected triaxial data (Castro correlation) in the plane  $CRR \cdot (1 - 5 \cdot E_{v,liq} / p_a)^{10}$  vs  $E_{s,liq}$  (c).

#### 4. Application of approaches 1 and 2 to literature data

In order to check the consistency of the previously exposed procedures, the two approaches have been applied to estimate the cyclic resistance of unsaturated soils for which experimental results are available in literature. In particular, triaxial tests results from Wang et al. [30] and from Okamura et al. [12] have been used. The previous ones have been obtained on the same Inagi sand tested in this work (at different degrees of saturation) and on Toyoura sand, while the results reported by Okamura et al. [12] have been obtained on a sand of a test site in the Kochi prefecture, Japan, hereafter simply called Kochi sand.

For completeness, some information on these soils are reported (soil gradings in Fig. 13, along with those of the three sands tested by Ref. [4]; on which eqs. (13a) and (15a) have been calibrated, and physical

properties in Table 3). Okamura et al. [12] do not provide the value of the specific gravity  $G_s$  for Kochi sand (see Table 3). In the calculations, the value  $G_s = 2.674$  (as calculated for SAS) was assumed. Considering the very little range of values of  $G_s$  for typical sands (see, for instance Table 1), this assumption is expected to have a minor effect on the results in terms of calculation of the specific volumetric and deviatoric components of the energy spent to liquefy.

##### 4.1. Approach 1

The values of  $\Delta CRR_{15}$  for the tests reported by Wang et al. [30] and from Okamura et al. [12] have been plotted in Fig. 14 along with the curve reported in Fig. 5, for triaxial tests. The good agreement of the literature data with the regression curve (eq. (13a)) obtained on the

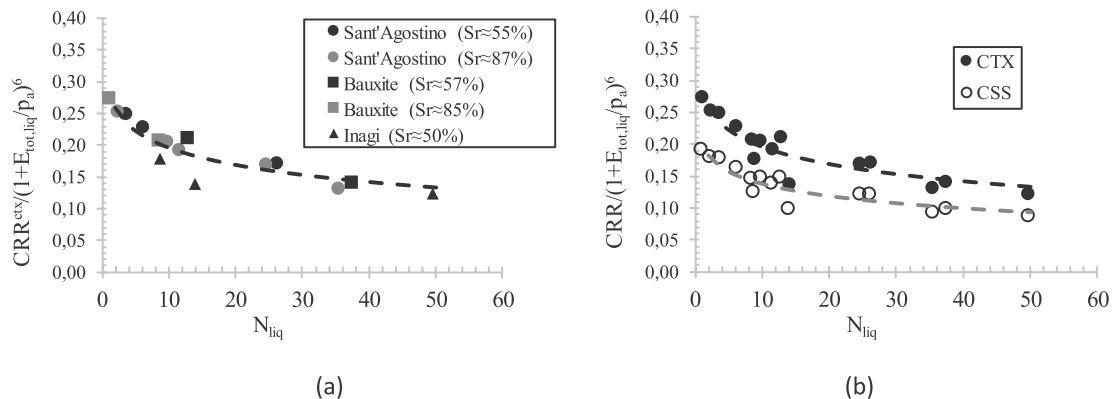


Fig. 12. Normalized cyclic resistance curve for cyclic triaxial tests (a); Normalized cyclic resistance curves for cyclic triaxial and corrected data (Castro correlation) (b).



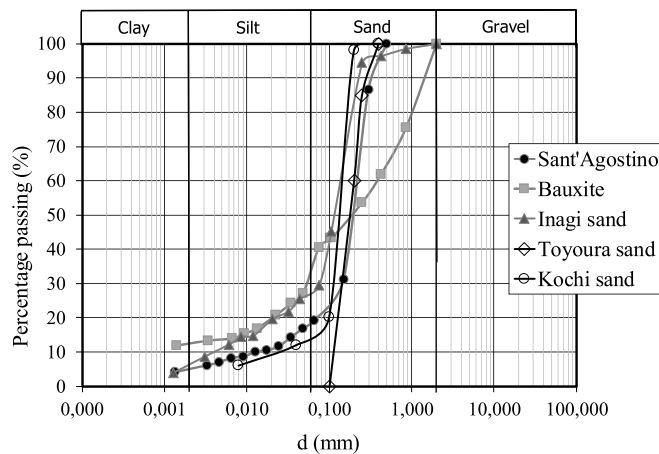


Fig. 13. Grain size distributions of the soils tested by Mele et al. [4] (Sant'Agostino, Bauxite, Inagi), Wang et al. [30] (Inagi and Toyoura) and Okamura et al. [12] (Kochi).

Table 3

Material properties of the soils (literature data) on which the two approaches have been checked. Properties of Inagi sand are not reported, as the same soil was tested by Mele et al. [4] and therefore the information are reported in Fig. 1.

Material Property	Toyourea sand <sup>a</sup>	Kochi sand <sup>b</sup>
Fines content (< 0.075 mm) %		15
Specific gravity, $G_s$	2.656	–
$D_{50}$ mm	0.20	0.15
$e_{max} - e_{min}$	0.898–0.611	–
$U_c$	1.90	5

<sup>a</sup> [30].

<sup>b</sup> [12].

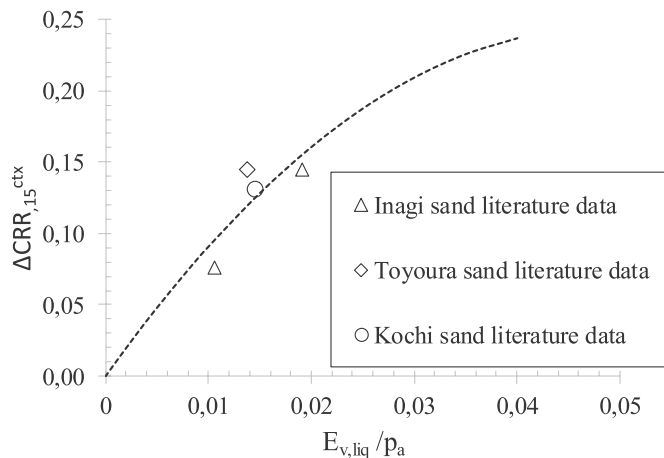


Fig. 14.  $\Delta CRR_{15}$  versus  $E_{v,liq}$ . Comparison of the proposed relationship (eq. (13a), Fig. 5) with the experimental results by Wang et al. [30] and by Okamura et al. [12].

results of Mele et al. [4] confirms that this approach is consistent. The cyclic resistance curves of these soils, given the specific testing state conditions (represented by  $E_{v,liq}$ ), have been obtained with approach 1 as described in §3 (Figs. 15 and 16). The curves interpret reasonably well the results obtained by Wang et al. [30] (Fig. 15), with some overestimation of  $CRR_{um}$  for Inagi sand, and a slight underestimation for Toyoura sand.

For Kochi sand (Fig. 16), the curve well fits the experimental results pertaining to the lower values of CRR, while it largely underestimates the result for the highest value (corresponding to the lowest value of

$N_{liq}$ ). This shows the major drawback of the use of approach 1: being based on a simple translation of the cyclic resistance curve ( $\Delta CRR$  does not depend on  $N_{liq}$ ) it is not able to catch the possible change of curvature of the unsaturated cyclic resistance curve. Furthermore, it may fail in the prediction of unsaturated cyclic resistance if applied out of the range of values of  $N_{liq}$  on which the saturated resistance curve was obtained (as is the case for Kochi sand reported in Fig. 16).

#### 4.2. Approach 2

Figs. 17 and 18 report the cyclic resistance curves obtained with approach 2, respectively to predict the experimental results by Wang et al. [30] and by Okamura et al. [12]. Both figures show that this modelling approach well fits the experimental results in unsaturated conditions, with a higher accuracy than approach 1.

### 5. Approaches 1 and 2 as induced partial saturation (IPS) design tools

The two procedures previously described can be used to predict the cyclic resistance of unsaturated soil in simple shear conditions and may be thus seen as relatively simple design tools to calculate the desired degree of saturation to be obtained via IPS for a given soil to increase its resistance to liquefaction.

Approach 1 is simpler to adopt, as it assumes that the liquefaction resistance curve related to a given degree of saturation can be obtained as a simple upwards translation of the one in saturation conditions. As previously discussed, the assumption that the  $CRR-N_{liq}$  curve does not change shape at different values of  $S_r$  is a strong simplification and must be adopted with extreme care. With all the experimental data adopted in this paper (the ones by Ref. [4]; on which the approach has been calibrated, and the ones by Refs. [12,30]), however, the approach seems to hold, at least in the range of values of  $N_{liq}$  of engineering interest (say  $N_{liq} < 20$ ). Likely, it will lack in accuracy for low or very low saturation degrees and higher  $N_{liq}$ . But these conditions are of little practical interest: because of the sharp increase of liquefaction resistance with just a little desaturation, IPS usually aims to reduce  $S_r$  to values not lower than 85%–90%.

Approach 2 needs a few calculation steps more than approach 1, being based on the calculation of the total specific energy and not only of its volumetric component. However, it has the advantage of not needing the knowledge of the saturated liquefaction resistance curve to predict the behaviour of the unsaturated soil. The result is not a translation of the  $CRR-N_{liq}$  curve, and any shape may be obtained, depending on the combination of specific volumetric and deviatoric energies to liquefaction. Approach 2 needs just the knowledge of the state parameters and of the soil water retention curve.

Comparing the simulations of independent experimental data reported in Figs. 15–18 for the two approaches, it can be noted that approach 2 better simulates the cyclic resistance of the three different sands. This is not surprising: being based on the calculation of the total specific energy spent to liquefy, it takes into account both the initial state conditions via the volumetric component, and cyclic damping via the deviatoric one (not considered by approach 1).

In the design of IPS, the goal is to find what degree of saturation  $S_r$  is needed to guarantee for the structures to protect a satisfactory performance with reference to serviceability and limit conditions with the desired safety margins, with reference to any kind of mechanism related to liquefaction [31]. In particular, two scenarios may be foreseen: one in which the risk is linked to the attainment of liquefaction (i.e. a temporary but total loss of stiffness and strength of the liquefied soil), and one in which the pore pressure build up may trigger limit states in the structures (e.g. bearing capacity failure or excessive settlements) before liquefaction is reached. In the first case, an increase of  $CRR^{css}$  for the given value of  $N_{eq}$  (which is the number of cycles corresponding to the design seismic action) is needed. In the second case (which may

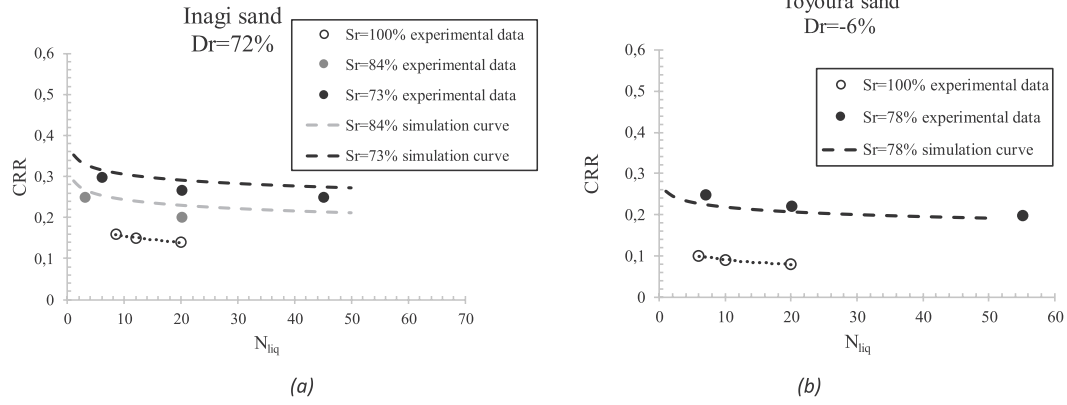


Fig. 15. Cyclic resistance curves of Inagi and Toyoura sand obtained with approach 1 along with the experimental data reported by Wang et al. [30] at different relative densities and at a confining stress of 60 kPa.

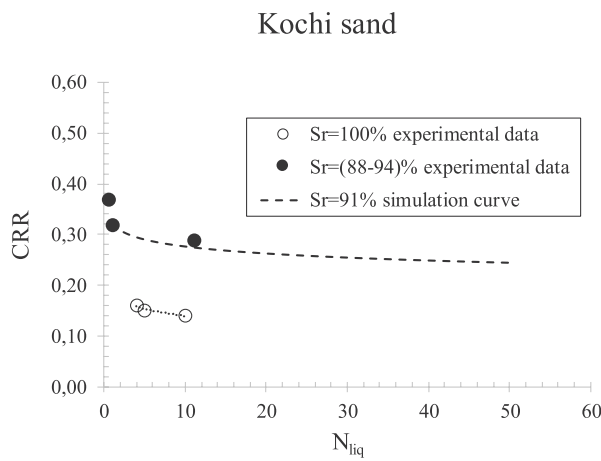


Fig. 16. Cyclic resistance curves of Kochi sand obtained with approach 1 along with the experimental data reported by Okamura et al. [12] at different relative densities and at a confining stress of 88 kPa.

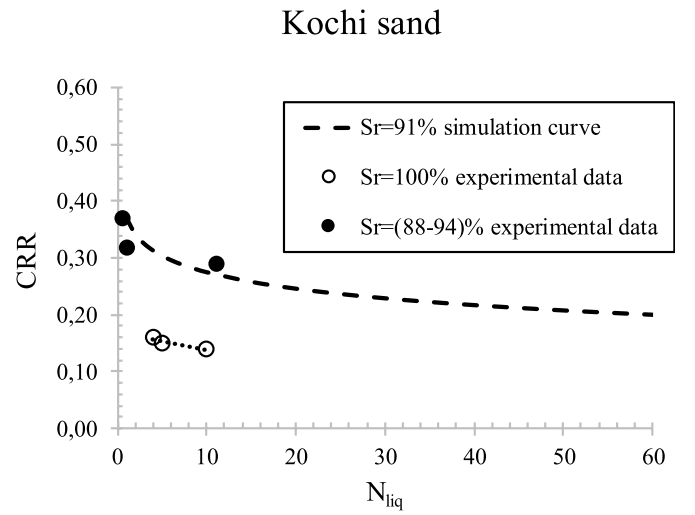


Fig. 18. Cyclic resistance curves of Kochi sand obtained with approach 2 (eq. (15a)) along with the experimental data reported by Okamura et al. [12] at different relative densities and at a confining stress of 88 kPa.

refer to situations in which the safety margins against liquefaction may be sufficient in saturated conditions), it is simply asked to have lower pore pressures for  $N=N_{eq}$ . Formally, this may be seen as the need to increase, for the given value of CSR, the value of  $N_{liq}$  to a higher value  $N_{liq}^*$ . Both scenarios ask for an increase of soil capacity via IPS to cope with seismic demand, and the two procedures depicted in Fig. 19 can be alternatively considered to this aim.

#### Increase CRR

The first procedure, on the left side of Fig. 19, refers to the need of increasing the safety factor against liquefaction. This means that the original safety margins are known (i.e., the saturated  $CRR^{ss}-N_{liq}$  curve is known). In this case, it is trivial to know what increment of

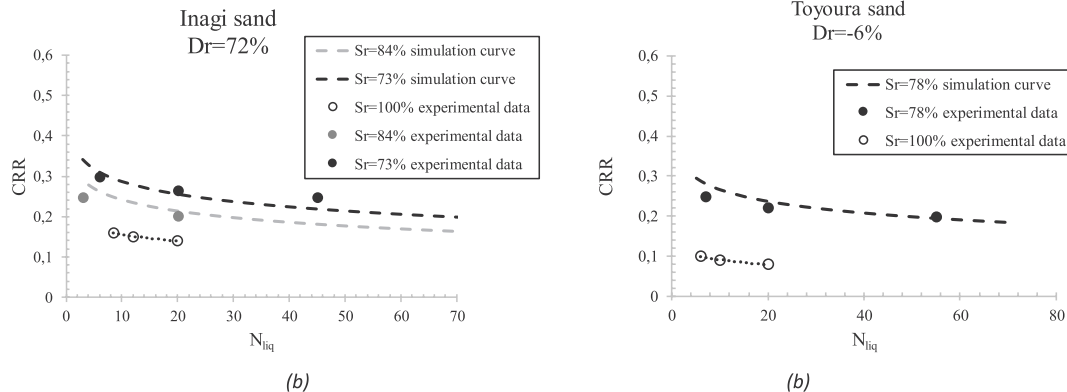
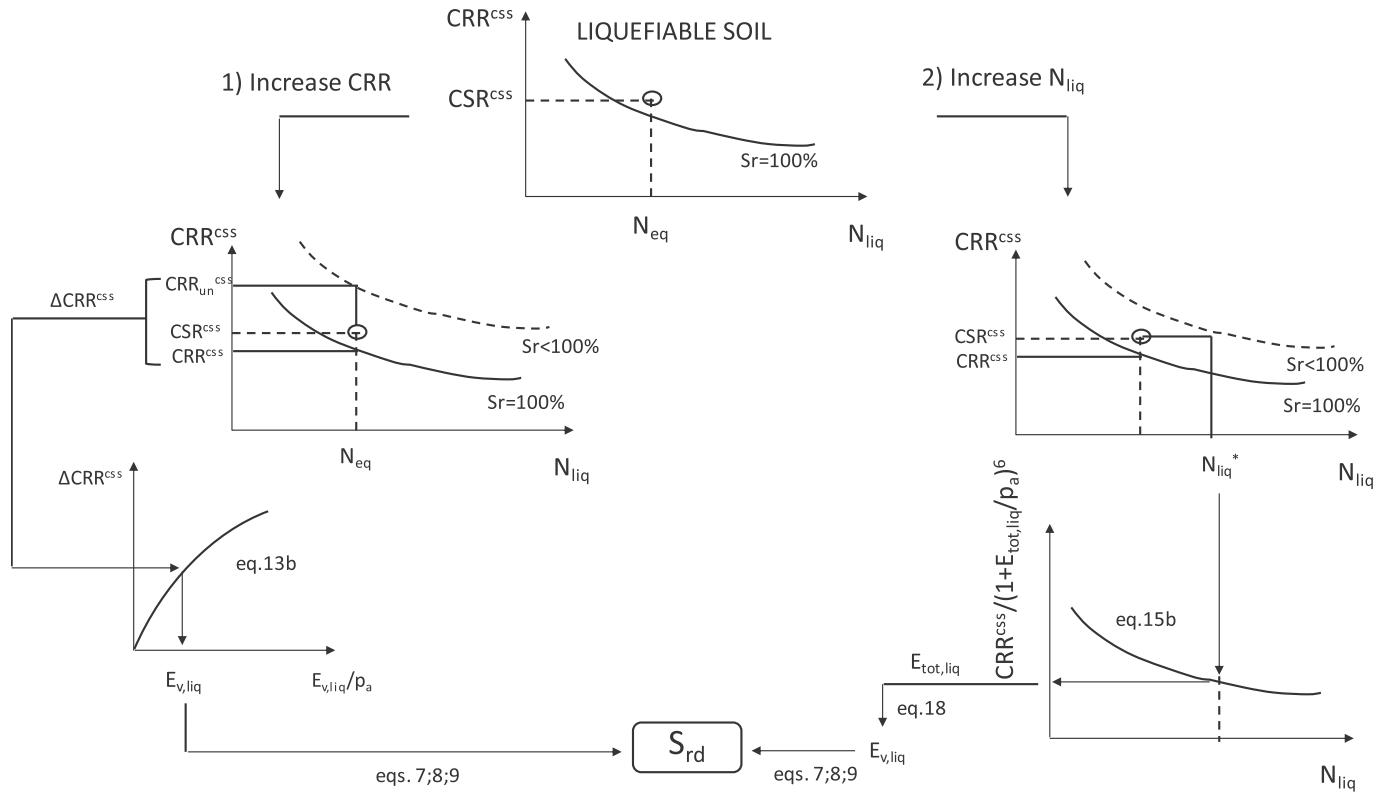


Fig. 17. Cyclic resistance curves of Inagi and Toyoura sand obtained with approach 2 (eq. (15a)) along with the experimental data reported by Wang et al. [30] at different relative densities and at a confining stress of 60 kPa.



**Fig. 19.** Possible procedures to calculate the degree of saturation needed to increment liquefaction resistance of sandy soils. The one on the left refers to Approach 1 (increase CRR); the one on the right to Approach 2 (increase  $N_{liq}$ ).

liquefaction resistance ( $\Delta CRR^{CSS}$ ) is needed once the desired safety margins are given, and therefore the previously proposed approach 1 is best suited as design tool. In fact, by knowing  $\Delta CRR^{CSS}$  it is possible to calculate  $E_{v,liq}$  (eq. (13b)). For high values of  $S_r$  (as will generally be the case for IPS), the contribution of  $E_{w,liq}$  is negligible. Therefore,  $E_{v,liq}$  can be considered as the sum of two components ( $E_{v,sk,liq}$  and  $E_{air,liq}$ ). Through an iterative procedure, the design value of  $S_r$  ( $S_{rd}$ ) can be finally calculated. Notwithstanding the limitations of approach 1 previously discussed, it has to be highlighted that  $N_{liq}$  is usually lower than 20, and thus its use is confined to the range of values of  $N$  on which it has been experimentally tested.

#### Increase $N_{liq}$

In this case, the seismic action (CSR) leads for  $N=N_{eq}$  to excessive pore pressures (but not to liquefaction). There is the need to reduce such pore pressures, regardless of the original safety margins against liquefaction. The saturated liquefaction resistance curve is not a necessary design tool in this case, being the design goal to increase  $N_{liq}$  till  $N_{liq}^*$ . The quantification of  $N_{liq}^*$  is out of the scope of this paper and will be discussed elsewhere. Generally speaking, it may be obtained once the maximum tolerable pore pressure  $u_{max}$  at  $N=N_{eq}$  has been evaluated with reference to the specific critical mechanism. In the case of bearing capacity failure triggered by pore pressure build up during seismic shaking, for instance, there are bearing capacity analytical formulations (e.g. Ref. [32] from which the value of  $u_{max}(N_{eq})$  at failure can be calculated. Then, using an analytical expression for the pore pressure build up curve  $u = u(N)$  (e.g. Ref. [33]) calibrated on such a value,  $N_{liq}^*$  is obtained.

In this case, approach 2 is best suited as design tool, as depicted on the right side of Fig. 19: once  $N_{liq}^*$  has been assigned, eq. (15b) allows to know the ratio  $CRR^{CSS}/(1+E_{tot,liq}/p_a)^6$  (considering in this case  $CRR^{CSS} = CSR$ ). The total specific energy to liquefaction  $E_{tot,liq}$  is the sum of two components  $E_{v,liq}$  and  $E_{s,liq}$ , where  $E_{s,liq}$  can be computed as

a function of CSR and  $E_{v,liq}$  (see Fig. 11b, eq. (14b)).  $E_{tot,liq}$  is therefore given by:

$$E_{tot,liq} = E_{v,liq} + 0.300 \cdot p_a \cdot e^{-23.7 \cdot CRR^{CSS}} \left(1 - 5 \cdot \frac{E_{v,liq}}{p_a}\right)^{10} \quad (18)$$

Using eq. (18), the design value  $S_{rd}$  can be calculated as done with approach 1 with a simple iterative procedure.

## 6. Conclusions

The laboratory results analysed in the paper allow to conclude that liquefaction resistance of unsaturated soils is strictly related to the specific energy spent to liquefaction. The volumetric component of such an energy univocally identifies the position of the  $CRR-N_{liq}$  curve in unsaturated conditions, once the position of the saturated one is known, and may be seen as a synthetic state variable. The deviatoric component is strictly related to the seismic action (CSR).

These experimental evidences have suggested two possible approaches to predict the liquefaction resistance of unsaturated soils, that may be seen as relatively simple design tools for IPS, with reference to different design goals. It has to be emphasized that the two approaches were calibrated on experimental results obtained in triaxial conditions on loose, fine sands with a very limited range of confining stresses ( $\approx 50$  kPa). However, they have been successfully tested on independent literature results also out of this range of state conditions: in fact, some of these results were obtained with a higher relative density ( $D_r = 72\%$ ) (namely Inagi sand [30]) or at higher confining stress (data from Ref. [12];  $\sigma_c = 88$  kPa).

Since the two approaches have been proposed by interpreting some experimental evidences, thus with an inductive procedure, further results are obviously needed to confirm their validity, and to check the possible effect of soil grading - which was not considered in this study - within the broad family of fine sands.

## Acknowledgements

This work was carried out as part of the European project Horizon 2020 – *Assessment and Mitigation of liquefaction potential across Europe: A holistic approach to protect structures infrastructures for improved resilience to earthquake – induced liquefaction disasters* – “LIQUEFACT” (grant agreement No. 700748).

## References

- [1] Chaney R. Saturation effects on the cyclic strength of sands. *Earthquake engineering and soil dynamics*. New York, NY, USA: American Society of Civil Engineers; 1978. p. 342–58.
- [2] Ishihara K, Tsukamoto Y, Nakazawa H, Kamada K, Huang Y. Resistance of partly saturated sand to liquefaction with reference to longitudinal and shear wave velocities. *Soils Found* 2002;42(No. 6):93–105.
- [3] Kobayashi M, Suemasa N, Katada T, Nagao K. Feasibility study on countermeasure against liquefaction using micro bubble. The twentieth international offshore and polar engineering conference. International Society of Offshore and Polar Engineers; 2010.
- [4] Mele L, Tan Tian J, Lirer S, Flora A, Koseki J. Liquefaction resistance of unsaturated sands: experimental evidence and theoretical interpretation. *Geotechnique* June 2019;69(6)<https://doi.org/10.1680/jgeot.18.P.042>.
- [5] Nakazawa H, Ishihara K, Tsukamoto Y, Kamata T. Case studies on evaluation of liquefaction resistance of imperfectly saturated soil deposits. *Proceedings of international conference on cyclic behaviour of soils and liquefaction phenomena*, bochum, Germany, vol. 31. 2004. p. 295–304.
- [6] Tsukamoto Y, Kawabe S, Matsumoto J, Hagiwara S. Cyclic resistance of two unsaturated silty sands against soil liquefaction. *Soils Found* 2014;54(6):1094–103.
- [7] Wang H, Koseki J, Sato T, Chiaro G, Tan Tian J. Effect of saturation on liquefaction resistance of iron ore fines and two sandy soils. *Soils Found* 2016;56(No. 4):732–44.
- [8] Yegian MK, Eseller-Bayat E, Alshawabkeh A, Ali S. Induced-Partial Saturation for liquefaction mitigation: experimental investigation. *J. Geotech. Geoenviron. Engng ASCE* 2007;133(No. 4):372–80.
- [9] Yoshimi Y, Yanaka K, Tokimatsu K. Liquefaction resistance of partially saturated sand. *Soils Found* 1989;29(No. 2):157–62.
- [10] Eseller-Bayat E, Yegian MK, Alshawabkeh A, Gokyer S. Prevention of liquefaction during earthquakes through induced partial saturation in sands. *Geotechnical engineering: new horizons*. Amsterdam: IOS Press; 2012. p. 188–94.
- [11] Nagao K, Suemasa N, Jinguuji M, Nakazawa H. July. In-situ applicability test of soil improvement for housing sites using Micro-Bubbles against soil liquefaction in URAYASU. The twenty-fifth international ocean and polar engineering conference. International Society of Offshore and Polar Engineers; 2015.
- [12] Okamura M, Takebayashi M, Nishida K, Fujii N, Jinguuji M, Imasato T, Yasuhara H, Nakagawa E. In-Situ desaturation test by air injection and its evaluation through field monitoring and multiphase flow simulation. *J. Geotech. Geoenviron. Engng ASCE* 2010;137(No. 7):643–52.
- [13] Mihalache C, Buscarnera G. Controllability criteria for soils saturated by a compressible fluid. *J. Eng Mech, ASCE* 2016;142(No. 10):04016076.
- [14] Bishop AW, Blight GE. Some aspects of effective stress in saturated and partly saturated soils. *Geotechnique* 1963;13(No. 3):177–97<https://doi.org/10.1680/geot.1963.13.3.177>.
- [15] Gallipoli D, Gens A, Vanet J, Romero E. Role of degree of saturation on the normally consolidated behavior of unsaturated soils. *Proc. 3rd int. Conf. On unsaturated soils*. 2002. p. 115–20.
- [16] Vanapalli SK, Fredlund DG, Pufahl DE, Clifton AW. Model for the prediction of shear strength with respect to soil suction. *Can Geotech J* 1996;33(3):379–92.
- [17] Wheeler SJ, Sharma RS, Bulson MSR. Coupling of hydraulic hysteresis and stress-strain behavior in unsaturated soils. *Geotechnique* 2003;53(1):41–54.
- [18] Gallipoli D, Gens A, Sharma R, Vaunat J. An elastoplastic model for unsaturated soil incorporating the effects of suction and degree of saturation on mechanical behaviour. *Geotechnique* 2003;53(1):123–35.
- [19] Okamura M, Soga Y. Effects of pore fluid compressibility on liquefaction resistance of partially saturated sand. *Soils Found* 2006;46(No. 5):695–700.
- [20] Desai CS. Evaluation of liquefaction using disturbed state and energy approaches. *J Geotech Geoenviron Eng* 2000;126(7):618–31.
- [21] Kokusho T. Liquefaction potential evaluations: energy-based method versus stress-based method. *Can Geotech J* 2013;50(10):1088–99.
- [22] Law KT, Cao YL, He GN. An energy approach for assessing seismic liquefaction potential. *Can Geotech J* 1990;27(3):320–9.
- [23] Azeiteiro RJ, Coelho PA, Taborda DM, Grazina JC. Energy-based evaluation of liquefaction potential under non-uniform cyclic loading. *Soil Dynam Earthq Eng* 2017;92:650–65.
- [24] Polito C, Green RA, Dillon E, Sohn C. Effect of load shape on relationship between dissipated energy and residual excess pore pressure generation in cyclic triaxial tests. *Can Geotech J* 2013;50(11):1118–28.
- [25] Baziar MH, Jafarian Y. Assessment of liquefaction triggering using strain energy concept and ANN model: capacity energy. *Soil Dynam Earthq Eng* 2007;27(12):1056–72.
- [26] Dief HM, Figueroa JL. Liquefaction assessment by the unit energy concept through centrifuge and torsional shear tests. *Can Geotech J* 2007;44(11):1286–97.
- [27] Green RA, Mitchell JK, Polito CP. An energy-based excess pore pressure generation model for cohesionless soils. *Proceedings of the John Booker memorial symposium*, Sydney Australia. Rotterdam, Netherlands: AA Balkema Publishers; 2000.
- [28] Polito CP, Green RA, Lee J. Pore pressure generation models for sands and silty soils subjected to cyclic loading. *J Geotech Geoenviron Eng* 2008;134(10):1490–500.
- [29] Castro G. Liquefaction and cyclic mobility of saturated sands. *J Geotech Eng Div, ASCE* 1975;101(No. GT6):551–69.
- [30] Wang H, Koseki J, Sato T. Resistance against liquefaction of unsaturated Toyoura sand and Inagi sand. *Bulletin of ERS* No 2014;47:2014.
- [31] Bray JD, Macedo J. Simplified procedure for estimating liquefaction-induced building settlement. *Proceedings of the 19th international conference on soil mechanics and geotechnical engineering*, Seoul 2017. 2017.
- [32] Karamitros DK, Bouckovalas GD, Chaloulos YK, Andrianopoulos KI. Numerical analysis of liquefaction-induced bearing capacity degradation of shallow foundations on a two-layered soil profile. *Soil Dynam Earthq Eng* 2013;44:90–101.
- [33] Chiaradonna A, Tropeano G, d'Onofrio A, Silvestri F. Development of a simplified model for pore water pressure build-up induced by cyclic loading. *Bulletin Earthquake Eng, BEE* 2018;16(No. 9):3627–52<https://doi.org/10.1007/s10518-018-0354-4>.

## List of notations

- CRR: cyclic resistance ratio  
 CRR<sub>s</sub>: cyclic resistance ratio required causing liquefaction at a fixed number of cycles in full saturation  
 CRR<sub>un</sub>: cyclic resistance ratio required causing liquefaction at a fixed number of cycles in partial saturation  
 CSR: cyclic stress ratio  
 D<sub>cyc</sub>: area of the cycle in the plane  $\epsilon_s$ - $q$   
 D<sub>c</sub>: degree of compaction  
 D<sub>r</sub>: relative density  
 D<sub>50</sub>: average particles size  
 e: void ratio index  
 E<sub>air,liq</sub>: specific energy of deformation of the air at liquefaction  
 e<sub>max</sub>: maximum void ratio  
 e<sub>min</sub>: minimum void ratio  
 e<sub>0</sub>: void ratio at the end of consolidation phase  
 E<sub>s</sub>: distortional specific energy  
 E<sub>s,liq</sub>: distortional specific energy at liquefaction  
 E<sub>s,sk,cyc</sub>: distortional specific energy of soil skeleton for each cycle  
 E<sub>s,sk,liq</sub>: distortional specific energy of soil skeleton at liquefaction  
 E<sub>tot</sub>: total specific energy of deformation  
 E<sub>tot,liq</sub>: specific energy of deformation needed to reach liquefaction  
 E<sub>v,liq</sub>: volumetric specific energy needed to reach liquefaction  
 E<sub>v,liq,ave</sub>: average volumetric specific energy needed to reach liquefaction  
 E<sub>v,sk,liq</sub>: volumetric specific energy of soil skeleton at liquefaction  
 E<sub>w,liq</sub>: specific energy of deformation of water at liquefaction  
 G<sub>s</sub>: specific gravity  
 N<sub>cyc</sub>: number of loading cycles  
 N<sub>eq</sub>: number of cycles corresponding to the design seismic action  
 N<sub>liq</sub>: number of cycles to reach liquefaction  
 N<sub>liq</sub><sup>\*</sup>: desired number of cycles to reach liquefaction  
 p<sub>a</sub>: atmospheric pressure  
 q<sub>d</sub>: cyclic deviatoric stress  
 q<sub>max</sub>: maximum deviatoric stress for each cycle  
 q<sub>min</sub>: minimum deviatoric stress for each cycle  
 R<sub>u</sub>: pore pressure ratio  
 s: suction (= u<sub>a</sub>-u<sub>w</sub>)  
 s<sub>liq</sub>: suction at liquefaction ( $\epsilon_{DA} = 5\%$ )  
 S<sub>r</sub>: degree of saturation  
 S<sub>rd</sub>: degree of saturation of design  
 S<sub>r,liq</sub>: degree of saturation when liquefaction occurs ( $\epsilon_{DA} = 5\%$ )  
 S<sub>ro</sub>: degree of saturation at the end of consolidation phase  
 u<sub>a</sub>: air pore pressure  
 u<sub>a,0</sub>: initial air pore pressure  
 u<sub>a,liq</sub>: air pore pressure when liquefaction occurs ( $\epsilon_{DA} = 5\%$ )  
 u<sub>w</sub>: water pore pressure  
 U<sub>c</sub>: coefficient of uniformity  
 ΔCRR: difference between CRR<sub>un</sub> and CRR<sub>s</sub> at a fixed number of cycles  
 Δu: excess pore pressure  
 ε<sub>a</sub>: axial strain  
 ε<sub>DA</sub>: axial strain (double amplitude)  
 ε<sub>s</sub>: deviatoric strain  
 ε<sub>v</sub>: volumetric strain  
 ε<sub>v,fin</sub>: volumetric strain at the end of cyclic test ( $\sigma'_{un} = 0$ )  
 ε<sub>v,liq</sub>: volumetric strain at liquefaction ( $\epsilon_{DA} = 5\%$ )  
 ρ<sub>a,liq</sub>: mass density of the air when liquefaction occurs ( $\epsilon_{DA} = 5\%$ )  
 ρ<sub>d</sub>: dry density of the soil  
 ρ<sub>d,max</sub>: maximum dry density of the soil  
 σ: total stress  
 σ<sub>liq</sub>: total stress at liquefaction  
 σ': effective stress  
 σ'<sub>c</sub>: effective confining stress at the end of consolidation  
 (σ-u<sub>a</sub>): net confining stress  
 σ'<sub>un</sub>: effective stress for unsaturated soil (Bishop notation)  
 σ'<sub>un,0</sub>: effective stress for unsaturated soil (Bishop notation) at the end of consolidation phase  
 σ'<sub>un,liq</sub>: effective stress for unsaturated soil (Bishop notation) when liquefaction occurs ( $\epsilon_{DA} = 5\%$ )  
 χ: Bishop's parameter